Reaction Wheel Design for CubeSats

Espen Oland and Rune Schlanbusch
Department of Scientific Computing, Electrical Engineering and Space Technology
Narvik University College
Narvik, Norway
{eol, runsch}@hin.no

Abstract— **This paper presents a reaction wheel design for CubeSats where it takes the limitation of size and mass into consideration. It presents an overview of which altitudes it is feasible to use magnetic torquers for momentum dumping as well as presenting equations for customizing reaction wheels for a CubeSat mission. The reaction wheels are then simulated for different CubeSat sizes and proved capable of performing attitude maneuvers. During these simulations a non-linear passivity-based sliding surface controller is used which through Lyapunov stability theory has been shown to be uniformly asymptotically stable.**

Keywords - Attitude Control; Reaction Wheel Design; CubeSat; Magnetic Torquers; Sliding Surface Controller;

I. Introduction

A 1 unit CubeSat is a satellite which is $10x10x10$ cm^3 large and weighs 1 kg. This results in strict limitations regarding actuation systems for CubeSats by eliminating many actuation systems and has made magnetic torquers one of the most used active actuation systems for CubeSats. Magnetic torquers work by sending current through a coil which produces a magnetic torque as it interacts with Earth's magnetic field. The magnetic field strength decreases proportional with the distance from the Earth, which makes magnetic torquers only applicable for low Earth orbits. In addition, the magnetic torquers lose control around one of the axes as the CubeSat passes the poles and the equator. This creates a need for a better actuation system designed for CubeSats.

One widely used actuation system is reaction wheels which mainly has been used for larger satellites, except for a few CubeSat missions. Reaction wheels operate by accelerating a wheel in one direction and thereby forcing the satellite to rotate in the other direction. Three reaction wheels can be mounted in an orthogonal system providing three axis control of a spacecraft.

A. Previous Work

Magnetic torquers have been flown on several CubeSats, while only a few CubeSats have implemented reaction wheels for attitude control. In [1] the BEESAT picosatellite is detailed which will be flown using three micro-reaction wheels together with magnetic torquers for attitude control. The total weight of their system is 0.105 kg and they are able to change the attitude 180 deg within three minutes. In [2] the design of an attitude control system using reaction wheels is discussed which is designed for the SwissCube picosatellite. The paper details a design guide regarding designing and manufacturing of inertia wheels for picosatellites.

A nonlinear sliding surface controller is presented in [3] and [4], and is developed based on [5], [6] and [7].

B. Contribution

In this paper we present the required mathematical models to determine size and mass of reaction wheels applicable for Cubesats. Through simulation results the reaction wheels are proven to be able to detumble CubeSats of varying sizes employing a nonlinear controller. The design has been tested on a 1 unit, 2 unit and 3 unit CubeSats, which provides comparative results which is of interest. Since magnetic torquers are the only feasible mechanism for momentum dumping of the reaction wheels, we also present a study of which altitudes that magnetic torquers can be used for momentum dumping.

II. Modeling

In the following, we denote by $\dot{\mathbf{x}}$ the time derivative of a vector $\mathbf{x}$, i.e. $\dot{\mathbf{x}} = d\mathbf{x}/dt$, and moreover, $\ddot{\mathbf{x}} = d^2\mathbf{x}/dt^2$. The cross product operator $\mathbf{a} \times \mathbf{b}$ is denoted $\mathbf{S}(\mathbf{a})\mathbf{b}$, $\boldsymbol{\omega}_{ba}^{c}$ is the angular velocity of frame a relative frame b, expressed in frame c, $\mathbf{R}_a^b$ is the rotation matrix from frame a to frame b, and $|\cdot|$ denotes the ℓ^2-norm. Coordinate reference frames are denoted by $\mathcal{F}_.$, with a subscript denoting reference frame. When the context is sufficiently explicit, we may omit the arguments of a function, vector or matrix.

A. Cartesian Coordinate Frames

The coordinate reference frames used throughout the paper are defined as follows:

Earth-centered inertial frame: The Earth-centered inertial (ECI) frame is denoted $\mathcal{F}_i$, and has its origin in the center of the Earth. The axes are denoted x_i, y_i, and z_i, where the z_i axis is directed along the axis of rotation of the Earth toward the celestial North Pole, the x_i axis is pointing in the direction of the vernal

978-1-4244-3628-6/09/$25.00 ©2009 IEEE

equinox, $\mathbf{Y}$, which is the vector pointing from the center of the sun toward the center of the Earth during the vernal equinox, and finally the y_i axis complete the right handed orthonormale frame.

Spacecraft orbit reference frame: The orbit frame, denoted $\mathcal{F}_o$, has its origin located in the center of mass of the spacecraft. The $\mathbf{e}_r$ axis in the frame coincide with the vector $\mathbf{r} \in \mathbb{R}^3$ from the center of the Earth to the spacecraft, and the $\mathbf{e}_h$ axis is parallel to the orbital angular momentum vector, pointing in the orbit normal direction. The $\mathbf{e}_\theta$ axis completes the right-handed orthogonal frame. The basis vectors of the frame can be defined as

$$\mathbf{e}_r := \frac{\mathbf{r}}{r} \qquad \mathbf{e}_\theta := \mathbf{e}_h \times \mathbf{e}_r \qquad \text{and} \quad \mathbf{e}_h := \frac{\mathbf{h}}{h} \tag{1}$$

where $\mathbf{h} = \mathbf{r} \times \dot{\mathbf{r}}$ is the angular momentum vector of the orbit, $h = |\mathbf{h}|$ and $r = |\mathbf{r}|$. This frame is also known as the Local Vertical/Local Horizontal (LVLH) frame.

Spacecraft body reference frame: The body frame of the spacecraft is denoted $\mathcal{F}_b$, and is located at the center of mass of the spacecraft, and its basis vectors are aligned with the principle axis of inertia.

B. Body Frame Rotation

Rotation between the previous mentioned orbit frame $\mathcal{F}_o$ to the body frame $\mathcal{F}_b$ may be described by

$$\mathbf{R}_o^b = \mathbf{I} + 2\eta\mathbf{S}(\boldsymbol{\epsilon}) + 2\mathbf{S}^2(\boldsymbol{\epsilon}) \tag{2}$$

and $\mathbf{q} = [\eta,\ \boldsymbol{\epsilon}^T]^T$ are the Euler parameters which satisfy the constraint $\eta^2 + \boldsymbol{\epsilon}^T\boldsymbol{\epsilon} = 1$. The matrix $\mathbf{S}(\cdot)$ is the cross product operator described as

$$\mathbf{S}(\boldsymbol{\epsilon}) = \boldsymbol{\epsilon}\times = \begin{bmatrix} 0 & -\epsilon_z & \epsilon_y \\ \epsilon_z & 0 & -\epsilon_x \\ -\epsilon_y & \epsilon_x & 0 \end{bmatrix}, \tag{3}$$

where $\boldsymbol{\epsilon} = [\epsilon_x,\ \epsilon_y,\ \epsilon_z]^T$. The inverse rotation can be performed by using the inverse conjugated of $\mathbf{q}$ as $\bar{\mathbf{q}} = [\eta,\ -\boldsymbol{\epsilon}^T]^T$.

C. Kinematics

The time derivative of equation (2) can be written as [8]

$$\dot{\mathbf{R}}_b^a = \mathbf{S}\left(\boldsymbol{\omega}_{ab}^a\right)\mathbf{R}_b^a = \mathbf{R}_b^a\mathbf{S}\left(\boldsymbol{\omega}_{ab}^b\right) \tag{4}$$

where $\boldsymbol{\omega}_{a,b}^a$ is the angular velocity of frame $\mathcal{F}_b$ relative to frame $\mathcal{F}_a$. The kinematic differential equations may be expressed as [8]

$$\dot{\mathbf{q}} = \mathbf{T}(\mathbf{q})\boldsymbol{\omega}_{ob}^b \tag{5}$$

where

$$\mathbf{T}(\mathbf{q}) = \frac{1}{2}\begin{bmatrix} -\boldsymbol{\epsilon}^T \\ \eta\mathbf{I} + \mathbf{S}(\boldsymbol{\epsilon}) \end{bmatrix}. \tag{6}$$

D. Dynamics

The dynamical model of the satellite can be described by a differential equation for angular velocity, and is deduced from Euler's equation of momentum. This equation describes the relationship between applied torque and angular momentum in a rigid body as [9]

$$\boldsymbol{\tau} = \dot{\mathbf{h}}_i = \dot{\mathbf{h}}_{ib}^b + \mathbf{S}(\boldsymbol{\omega}_{ib}^b)\mathbf{h}_{ib}^b = \mathbf{J}\dot{\boldsymbol{\omega}}_{ib}^b + \mathbf{S}(\boldsymbol{\omega}_{ib}^b)\mathbf{J}\boldsymbol{\omega}_{ib}^b, \tag{7}$$

where $\boldsymbol{\tau} \in \mathbb{R}^3$ is the total torque working on the body frame, where subscript i indicates inertial frame and subscript b indicates the body frame. Angular velocity is denoted $\boldsymbol{\omega}$, and $\mathbf{J}$ is the moment of inertia. The torque working on the body is derived from two parameters, where $\boldsymbol{\tau}_d^b$ is the disturbance torque and $\boldsymbol{\tau}_a^b$ is the actuator torque such as

$$\boldsymbol{\tau} = \boldsymbol{\tau}_a^b + \boldsymbol{\tau}_d^b. \tag{8}$$

The dynamical model is derived from (7) and (8) expressed as

$$\boldsymbol{J}\dot{\boldsymbol{\omega}}_{ib}^b = -\mathbf{S}(\boldsymbol{\omega}_{ib}^b)\mathbf{J}\boldsymbol{\omega}_{ib}^b + \boldsymbol{\tau}_a^b + \boldsymbol{\tau}_d^b, \tag{9}$$

where $\boldsymbol{\omega}_{ib}^b$ is the angular velocity of the body frame relative to the inertial reference system, and the angular velocity of the body frame relative to the orbit frame, $\boldsymbol{\omega}_{ob}^b$ is expressed as

$$\boldsymbol{\omega}_{ob}^b = \boldsymbol{\omega}_{ib}^b - \mathbf{R}_o^b\boldsymbol{\omega}_{io}^o, \tag{10}$$

where

$$\boldsymbol{\omega}_{io}^o = \mathbf{R}_i^o\frac{\mathbf{S}(\mathbf{r})\mathbf{v}}{\mathbf{r}^T\mathbf{r}}. \tag{11}$$

III. Reaction Wheel Design

When designing reaction wheels for CubeSats there are two major limitations, volume and mass. In the following design the reaction wheels are designed weighing 0.050 kg each and with a maximum diameter of 40.2 mm and with a height of 10 mm. By leaving 8 mm for casing and assuming that there is a motor that can fit within the boundaries of the reaction wheel, the total size of one reaction wheel would have a diameter of 50 mm and a height of 15 mm. The reaction wheels are designed with an ring along the periphery of the wheel where most of the mass is placed, which reduces the total weight while maintaining a high level of momentum. With the size and mass as limiting factors, the total mass of one reaction wheel can be decomposed into

$$m_{\text{total}} = m_{\text{disk}} + m_{\text{ring}} = 0.05 \text{ kg} \tag{12}$$

where the mass of each reaction wheel can be found by using the expression for mass of a cylinder and a ring as

$$m_{total} = \rho\pi r_{\text{disk}}^2 h_{\text{disk}} + \rho\pi(r_{\text{ring}}^2 - r_{\text{disk}}^2)h_{\text{ring}}, \tag{13}$$

where ρ is the density of the material, r is the radius and h is the height. By selecting iron which has a density of $7.85 \cdot 10^3$ kg/m^3, (12) can be solved for the

TABLE I
DESIGN PARAMETERS

Parameter	Value
r_{disc} [mm]	15
r_{ring} [mm]	20.1
h_{disc} [mm]	1
h_{ring} [mm]	10
m_{disc} [kg]	0.0055
m_{ring} [kg]	0.0445

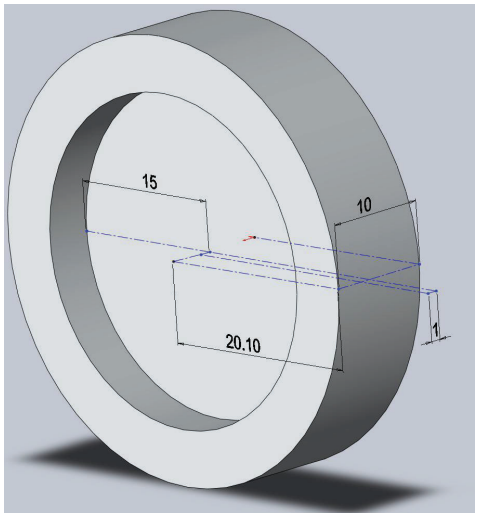

Fig. 1. Reaction Wheel Design, (Dimensions are in mm)

ring radius by using (13). The disk radius is chosen as 15 mm and with a total height of 1 mm while the height of the ring is chosen to be 10 mm. This results in

$$7.85 \cdot 10^3 \pi \cdot 0.015^2 \cdot 0.001 \quad (14)$$
$$+7.85 \cdot 10^3 \pi (r_{\text{ring}}^2 - 0.015^2) \cdot 0.01 = 0.05$$

where r_{ring} is the radius of the ring and is found to be 20.1 mm. The dimensions of the reaction wheel are shown in Fig. 1 and the design parameters are summarized in Table I. Assuming that one motor weigh 0.015 kg, the total weight of a three axis reaction wheel system would be 0.195 kg.

With the known design parameters, we find the inertial momentum for the reaction wheel as [10]

$$I_{\text{disk}} = \frac{m_{\text{disk}} r_{\text{disk}}^2}{2} = \frac{0.0055 \cdot 0.015^2}{2} = 6.1875 \cdot 10^{-7}, \quad (15)$$

and

$$I_{\text{ring}} = \frac{m_{\text{ring}}(r_{\text{ring}}^2 + r_{\text{disk}}^2)}{2} \quad (16)$$
$$= \frac{0.0445(0.0201^2 + 0.015^2)}{2} = 1.34 \cdot 10^{-5},$$

which produces a total inertial for each reaction wheel of

$$I_{\text{total}} = I_{\text{disk}} + I_{\text{ring}} = 1.46 \cdot 10^{-5} \text{ kgm}^2. \quad (17)$$

TABLE II
REACTION WHEEL ROTATION TIME

	1 Unit	2 Unit	3 Unit
I_{xx}, [kgm^2]	$1.67 \cdot 10^{-3}$	$8.33 \cdot 10^{-3}$	$25 \cdot 10^{-3}$
I_{yy}, [kgm^2]	$1.67 \cdot 10^{-3}$	$8.33 \cdot 10^{-3}$	$25 \cdot 10^{-3}$
I_{zz}, [kgm^2]	$1.67 \cdot 10^{-3}$	$3.33 \cdot 10^{-3}$	$5 \cdot 10^{-3}$
Time to Rotate 90°, [s]	1.4990	7.4770	22.4399

By selecting a motor with a maximum wheel speed of 13700 rpm the maximum angular momentum can be found as [9]

$$h_{\max} = I_{\text{total}} \omega_{\max} = 1.46 \cdot 10^{-5} \cdot 13700 \cdot \frac{2\pi}{360} = 0.0035. \quad (18)$$

The total angular rotation θ produced by a reaction wheel within a given time t_f is given by [9]

$$t_f = \frac{2 I_{\max} \theta}{h_{\max}} \quad (19)$$

where $I_{\max}$ is the greatest inertia of the satellite. Equation (19) can be solved for each of the three CubeSat sizes giving an indication of the time required to rotate the satellite 90° and is shown in Table II.

IV. PERTURBATIONS

Aerodynamic Torque: Aerodynamic forces in near-Earth orbit leads to drag and reduces the altitude over time. These forces that act on the spacecraft body and can be presented as [11]

$$\mathbf{f}_{\text{atm}}^s = \mathbf{C}_a^s \begin{bmatrix} 0 \\ -\frac{1}{2}\rho v^2 C_d A \\ 0 \end{bmatrix} \quad (20)$$

where ρ is the atmospheric density, $v = |\mathbf{v}|$ is the spacecraft velocity, C_d is the drag coefficient which is 1.07 for a cube [12] and A is the equivalent spacecraft surface in the motion direction and $\mathbf{C}_a^s$ is the orbit frame transformation matrix defined as [11]

$$\mathbf{C}_a^s = \frac{h}{pv} \begin{bmatrix} \frac{p}{r} & e \sin \nu & 0 \\ -e \sin \nu & \frac{p}{r} & 0 \\ 0 & 0 & \frac{pv}{h} \end{bmatrix}. \quad (21)$$

h is the angular momentum, p is the semi-latus rectum, ν is the true anomaly and e is the eccentricity of the orbit.

Gravity Gradient Torque: A spacecraft in low orbit does not experience the same gravitational pull on all parts of its body, which causes the spacecraft to turn towards the Earth in accordance with the principal axis of inertia. According to [11] the torque can be expressed as

$$\boldsymbol{\tau}_d = \frac{3\mu}{\mathbf{r}^5} \mathbf{S}(\mathbf{r}) \mathbf{J} \mathbf{r}, \quad (22)$$

where μ is the geocentric gravitational constant.

Solar Radiation Torque: The torque produced when radiation and particles from the Sun hits the satellite body can be found as a scalar by [13]

$$\tau_s = F(c_p - c_g) \quad \text{and} \quad F = \frac{F_s}{c} A_s (1+q)\cos\beta, \quad (23)$$

where $F_s = 1367\ \mathrm{W/m^2}$ is the solar constant, c is the speed of light, A_s is the surface area, c_p is the center of pressure, c_g is the center of gravity, $q \in [0,1]$ is the reflectance factor while β is the incidence angle of the Sun.

Magnetic Field: Electronics inside the satellite may result in a residual magnetic dipole which will interact with Earth's magnetic field. The torque produced as this field interacts with Earth's magnetic field can be found as [13]

$$\tau_m = DB, \quad (24)$$

where D is the residual dipole of the satellite and B is the Earth's magnetic field.

V. Momentum Dumping

As the perturbing forces are acting on the satellite body, the reaction wheels will accelerate constantly to counteract these forces. This acceleration will continue until the reaction wheels become saturated, where they no longer are able to perform attitude maneuvering. The excess momentum must be unloaded and can be done in a momentum dumping scheme which mainly can be done for CubeSats by using magnetic torquers. As the magnetic torquers produce torque in one direction, a reaction wheel can be decelerated producing a net torque of zero. This can be done for all the reaction wheels, and is mainly limited by the torque produced by the magnetic torquers which decreases the further away from the Earth the spacecraft is. According to [9] the magnetic field strength decreases as

$$B^b = \frac{m_d}{r^3} \quad (25)$$

where $m_d = 7.96 \cdot 10^{15}$ Wbm is the magnetic dipole strength and r is the distance from the center of the Earth.

In order for the magnetic torquers to be able to perform momentum dumping of the reaction wheels, they must produce a higher torque than the current perturbing forces that exist in an orbit. With 150 mW available power for the each of the torquers and with a supply voltage of 3.7V the current for the the three coils can be calculated to be $i_c = 40.5$ mA and inserted into

$$\mathbf{m}^b = \mathbf{i}_c \mathbf{N} \mathbf{A} \quad (26)$$

where A is the coil area, N is the number of turns for the coils. By using (26) with coils of 100 turns and an area of $0.00757\mathrm{m}^2$ the total magnetic moment can be calculated to be $0.0306585\ \mathrm{Am}^2$. The magnetic moment can be used to find the torque produced by the magnetic torquers as

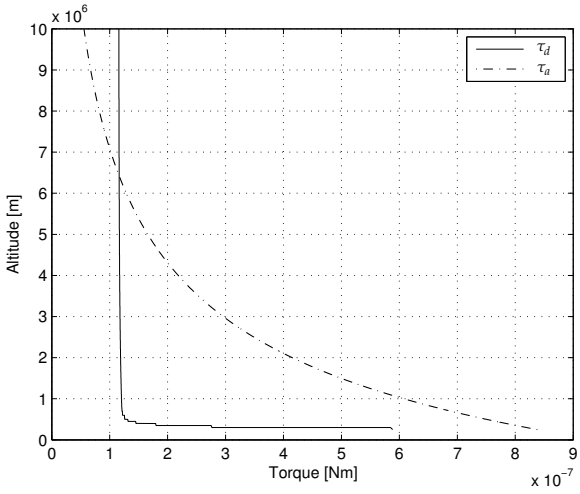

Fig. 2. Magnetic Torque vs. Perturbing forces for a 1 unit CubeSat

$$\boldsymbol{\tau}_a^b = \mathbf{m}^b \times \mathbf{B}^b, \quad (27)$$

which can be written as a scalar [9]

$$\tau_a^b = m^b B^b \sin(\alpha), \quad (28)$$

where α is the angle between Earth's magnetic field and the magnetic moment produced by a magnetic torquer. By assuming a perfect case where the torquer is normal to the magnetic field and inserting (25) into (28) we obtain

$$\tau_a^b = \frac{m^b m_d}{r^3}. \quad (29)$$

Equation (29) can be plotted together with the sum of perturbing forces as functions of altitude which can be used to show the maximum altitude for magnetic torquers as a momentum dumping device.

The total perturbing forces acting on the satellite body can be found by adding them together, where the gravity gradient can be found from (22), the solar radiation can be assumed to be constantly equal to $1.5371 \cdot 10^{-8}$ [13] while the internal magnetic field can be assumed to produce a disturbance torque of $1 \cdot 10^{-6}$. The atmospheric drag can be found from (20) using atmospheric densities as stated in [14] and assume a worst case where the center of mass is 2 cm from the geometric center of the cube [15]. This is shown in Fig. 2 and it can be seen that for altitudes higher than 6242 km, the perturbing forces are larger than the produced magnetic torque, and thus it is not possible to use magnetic torquers for momentum dumping above this altitude.

Note that since all the CubeSat sizes are limited by one side of $10x10\ \mathrm{cm}^2$, Fig. 2 is applicable for three units as at least one axis will have a magnetic torquer constrained by this area.

VI. Controller Design

For control of the spacecraft attitude, we incorporate a passivity based sliding surface controller as in [16], similar to the one derived in [4]. For the control law it is assumed that the spacecraft has available information of its orbit position $\mathbf{r}$, orbit velocity $\mathbf{v}$, attitude $\mathbf{q}$, and angular velocity $\boldsymbol{\omega}_{i,b}^{b}$.

A. Problem Formulation

The control problem is to design a controller that makes the state $\mathbf{q}(t)$ converge towards the generated reference specified as $\mathbf{q}_d$ satisfying the kinematic equation (5) and acts as a solution to the dynamic model presented in (9). The error quaternion $\tilde{\mathbf{q}} = [\tilde{\eta},\ \tilde{\boldsymbol{\epsilon}}^\top]^\top$ is found by using the quaternion product

$$\tilde{\mathbf{q}} = \mathbf{q} \otimes \bar{\mathbf{q}}_d = \frac{1}{2}\begin{bmatrix} \eta\eta_d + \boldsymbol{\epsilon}^\top\boldsymbol{\epsilon}_d \\ \eta_d\boldsymbol{\epsilon} - \eta\boldsymbol{\epsilon}_d - \mathbf{S}(\boldsymbol{\epsilon})\boldsymbol{\epsilon}_d \end{bmatrix}, \tag{30}$$

and the error dynamic can according to [17] be expressed as

$$\dot{\tilde{\mathbf{q}}} = \frac{1}{2}\mathbf{T}(\tilde{\mathbf{q}})\tilde{\boldsymbol{\omega}}.$$

Due to the redundancy in the quaternion representation, $\tilde{\mathbf{q}}$ and $-\tilde{\mathbf{q}}$ represent the same physical attitude but mathematically it differs by a 2π rotation about an arbitrary axis. Therefore we are not able to achieve global representation since the term global refers to the whole state space $\mathbb{R}^n$ according to [18]. Since both equilibrium points represent the same physical representation we choose the equilibrium point which require the shortest rotation, minimizing the path length. Hence $\tilde{\mathbf{q}}_+ = [1,\ \mathbf{0}^\top]^\top$ is chosen if $\tilde{\eta} \leq 0$, and $\tilde{\mathbf{q}}_- = [-1,\ \mathbf{0}^\top]^\top$ is chosen if $\tilde{\eta} < 0$. For the positive equilibrium point, the attitude error vector is chosen as [19] $\tilde{\mathbf{e}}_{q+} = [1 - \tilde{\eta},\ \tilde{\boldsymbol{\epsilon}}^\top]^\top$, while for the negative equilibrium point, the error vector is chosen as $\tilde{\mathbf{e}}_{q-} = [1 + \tilde{\eta},\ \tilde{\boldsymbol{\epsilon}}^\top]^\top$. The angular velocity error vector is chosen as $\mathbf{e}_\omega = \boldsymbol{\omega} - \boldsymbol{\omega}_d$.

B. Control Law

In the following $\mathbf{e}_q = \mathbf{e}_{q+}$, and we defined a reference frame as

$$\boldsymbol{\omega}_r = \boldsymbol{\omega}_d - \boldsymbol{\Gamma}\boldsymbol{\Lambda}_e^T(\mathbf{e}_q)\mathbf{e}_q, \tag{31}$$

where the desired trajectory for pointing is defined as $\mathbf{q}_d(t)$ and $\boldsymbol{\omega}_d(t)$ with the relationship using equation (5), $\boldsymbol{\Gamma} = \boldsymbol{\Gamma}^T > 0$, $\boldsymbol{\Lambda}_e(\mathbf{e}_{\pm q}) = \mathbf{T}(\mathbf{q})$ and using the rotation error expressed in (30). We then define a sliding surface by using equation (31) which leads to

$$\mathbf{s} = \boldsymbol{\omega} - \boldsymbol{\omega}_r = \mathbf{e}_\omega + \boldsymbol{\Gamma}\boldsymbol{\Lambda}_e^T\mathbf{e}_q. \tag{32}$$

By using a control law expressed as

$$\boldsymbol{\tau}_a = \mathbf{J}\dot{\boldsymbol{\omega}}_r - \mathbf{S}\left(\mathbf{J}\boldsymbol{\omega}\right)\boldsymbol{\omega}_r - \boldsymbol{\tau}_d - \mathbf{K}_p\boldsymbol{\Lambda}_e^T\mathbf{e}_q - \mathbf{K}_d\mathbf{s}, \tag{33}$$

where $\mathbf{K}_p = \mathbf{K}_p^T > 0$ and $\mathbf{K}_d = \mathbf{K}_d^T > 0$ are feedback gain matrixes, we obtain the closed-loop system by inserting (33) into (9)

$$\mathbf{J}\dot{\mathbf{s}} - \mathbf{S}\left(\mathbf{J}\boldsymbol{\omega}\right)\mathbf{s} + \mathbf{K}_p\boldsymbol{\Lambda}_e^T\mathbf{e}_q + \mathbf{K}_d\mathbf{s} = \mathbf{0}. \tag{34}$$

TABLE III
Simulation Values and Results

Parameters	Values		
Initial Euler Angles, [°]	45	20	−30
Desired Euler Angles, [°]	0	0	0
Initial Angular Rates, [rad/s]	0.01	0.02	−0.03
Sliding Surface, Γ	1		
Sliding Surface, K_p	1		
Sliding Surface, K_d	2		
Motor Wheel Speed, [rpm]	13700		
Motor Torque Constant	$0.866 \cdot 10^{-3}$		
Parameters	**1 Unit**	**2 Unit**	**3 Unit**
Attitude Maneuver Time, [s]	20	75	210
Attitude Accuracy, [°]	0.0067	0.00116	0.00108

A radial unbounded, positive definite Lyapunov function candidate is defined as

$$V = \frac{1}{2}\mathbf{s}^T\mathbf{J}\mathbf{s} + \frac{1}{2}\mathbf{e}_q^T\mathbf{K}_p\mathbf{e}_q > 0 \quad \forall \ \ \mathbf{s} \neq \mathbf{0},\ \mathbf{e}_1 \neq \mathbf{0}, \tag{35}$$

which through differentiation and insertion of (34) leads to (*cf.*[16])

$$\dot{V} = -\mathbf{s}^T\mathbf{K}_d\mathbf{s} - \mathbf{e}_q^T\boldsymbol{\Lambda}_e\boldsymbol{\Gamma}\mathbf{K}_p\boldsymbol{\Lambda}_e^T\mathbf{e}_q. \tag{36}$$

By employing Lyapunov arguments (*cf.* [20]), we find that the closed-loop system in equation (34) is uniformly asymptotically stable (UAS) in the equilibrium point $(\mathbf{e}_q, \mathbf{e}_\omega) = (\mathbf{0}, \mathbf{0})$. The proof for the negative equilibrium point $\mathbf{e}_{q-}$ is performed in the same way leading to a similar result. Hence, it followes that the dual equilibrium points $(\mathbf{e}_{q\pm}, \mathbf{e}_\omega) = (\mathbf{0}, \mathbf{0})$ are UAS, thus we do not obtain global results.

VII. Simulations

The simulations are performed using a circular orbit of 500 km altitude and with 79° inclination. It is assumed that no perturbing forces are acting on the satellite body and it is shown that each of the three CubeSat sizes are able to stabilize the satellite using the designed reaction wheels. The simulation results are shown in Fig. 3-5 where the 1U CubeSat is the quickest satellite to detumble and stabilize its attitude, while the 3U requires the longest time. It is seen that the 3U CubeSat has the lowest attitude error while the 1U has the highest attitude error. Both the detumbling time and the attitude error are direct results of the different moments of inertia of the three CubeSats as is shown in Table III.

VIII. Conclusions

In this paper we have presented a detailed design of reaction wheels for CubeSats. We have also presented a passivity-based sliding surface controller which was proven UAS, and was implemented in simulations of three different CubeSats using the proposed reaction wheels. The simulations showed that the controller performed well during attitude maneuvers and that the

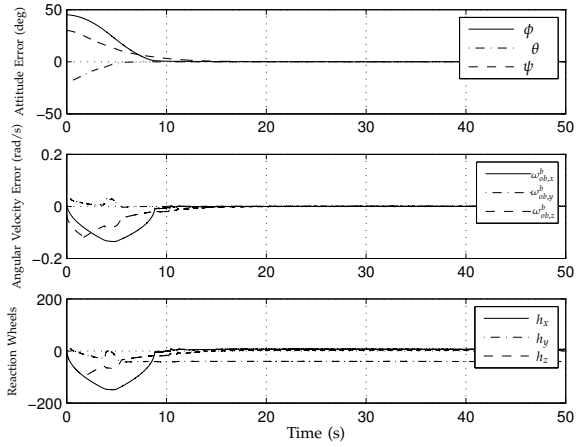

Fig. 3. Simulation with a 1 Unit CubeSat

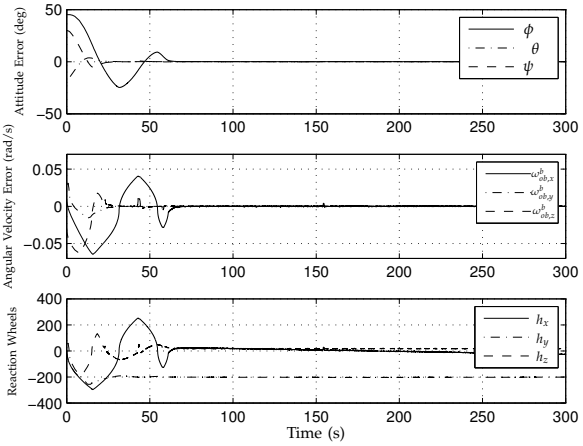

Fig. 4. Simulation with a 2 Unit CubeSat

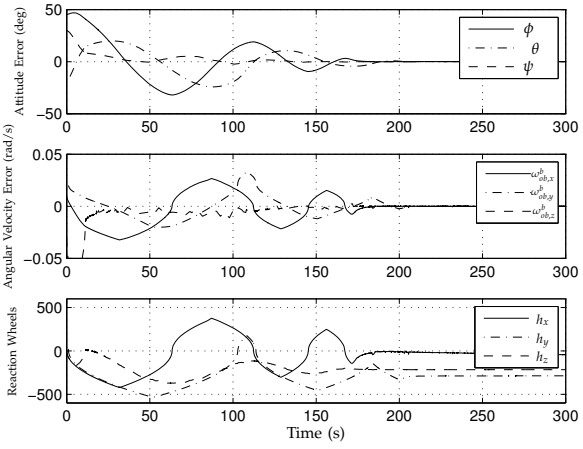

Fig. 5. Simulation with a 3 Unit CubeSat

reaction wheels were able to maintain a high level of attitude control as well as stabilize the satellites within a reasonable time.

Acknowledgment

The authors would like to thank Tom Stian Andersen for his help in creating the 3D model of the reaction wheels.

References

[1] Kayal, H., Baumann, F., and Briess, K., "BEESAT - A Pico Satellite of TU Berlin for the In-Orbit Verification of Miniaturised Wheels," *International Astronautical Conference*, 2008.

[2] Bozovic, G., "SwissCube: development of an ultra-light and efficient Ineria Wheel for the attitude control and stabilization of CubeSat class satellites," *International Astronautical Conference*, 2008.

[3] Slotine, J. J.-E. and Li, W., "On the adaptive control of robot manipulators," *International Journal of Robotics Research*, Vol. 6, 1987, pp. 49–59.

[4] Slotine, J. J.-E. and Li, W., *Applied Nonlinear Control*, Prentice Hall, New Jersey, US, 1991.

[5] Takegaki, M. and Arimoto, S., "A new feedback method for dynamic control of manipulators," *ASME Journal of Dynamical Systems, Measurement and Control*, Vol. 102, 1981, pp. 119–125.

[6] Berghuis, H. and Nijmeijer, H., "A Passivity Approach to Controller-Observer Design for Robots," *IEEE Transactions on Robotics and Automation*, Vol. 9, No. 6, 1993, pp. 740–754.

[7] Paden, B. and Panja, R., "Globally asymptotically stable 'PD+' controller for robot manipulators," *International Journal of Control*, Vol. 47, No. 6, 1988, pp. 1697–1712.

[8] Egeland, O. and Gravdahl, J. T., *Modeling and Simulation for Automatic Control*, Marine Cybernetics, Trondheim, Norway, 2002.

[9] Sidi, M. J., *Spacecraft Dynamics and Control*, Cambridge University Press, New York, 1997.

[10] Young, H. D. and Freedman, R. A., *University Physics, 11th Edition*, Pearson Education, 2004.

[11] Schaub, H. and Junkins, J. L., *Analytical Mechanics of Space Systems*, AIAA Education Series, American Institute of Aeronautics and Astronautics, Reston, VA, 2003.

[12] White, F., *Fluid Mechanics, Second Edition*, Mechanical Engineering Series, Mcgraw-Hill International Editions, 1986.

[13] Gravdahl, J., Eide, E., Skavhaug, A., Fauske, K. M., Svartveit, K., and Indergaard, F. M., "Three Axis Attitude Determination and Control System for a Picosatellite: Design and Implementation," *Proceedings of the 54th International Astronautical Congress*, Bremen, Germany, 2003.

[14] Wertz, J. R., editor, *Spacecraft Attitude Determination and Control*, Kluwer Academic Publishers, London, 1978.

[15] Lee, S., Hutputanasin, A., Toorian, A., Lan, W., and Munakata, R., "Cubesat Design Specification," Tech. rep., California Polytechnic State University, 2008.

[16] Schlanbusch, R., Reiten, K., Kristiansen, R., and Nicklasson, P. J., "Passivity-Based Attitude Control of the SSETI ESMO Satellite," *International Lunar Conference*, 2007.

[17] Fjellstad, O.-E., *Control of Unmanned Underwater Vehicles in Six Degrees of Freedom*, Ph.D. thesis, Department of Engineering Cybernetics, Norwegian University of Science and Technology, Trondheim, Norway, 1994.

[18] Hahn, W., *Stability of Motion*, Springer-Verlag, Berlin, Germany, 1967.

[19] Kristiansen, R., *Dynamic Synchronization of Spacecraft - Modeling and Coordinated Control of Leader-Follower Spacecraft Formations.*, Ph.D. thesis, Department of Engineering Cybernetics, Norwegian University of Science and Technology, Trondheim, Norway, 2008.

[20] Khalil, H. K., *Nonlinear Systems, third edition*, Pearson Education International Inc., Upper Saddle River, New Jersey, USA, 2002.